Cell surface proteoglycan-mediated uptake and accumulation of the Alzheimer's disease peptide Aβ(1–42)

BBA - Biomembranes 1860 (2018) 2204–2214

Contents lists available at ScienceDirect

BBA - Biomembranes

journal homepage: www.elsevier.com/locate/bbamem

Cell surface proteoglycan-mediated uptake and accumulation of the Alzheimer's disease peptide Aβ(1–42)

Emelie Wesén[a], Audrey Gallud[a], Alexandra Paul[a], David J. Lindberg[a], Per Malmberg[b], Elin K. Esbjörner[a,*]

[a] Division of Chemical Biology, Department of Biology and Biological Engineering, Chalmers University of Technology, Kemivägen 10, 412 96 Gothenburg, Sweden
[b] Division of Chemistry and Biochemistry, Department of Chemistry and Chemical Engineering, Chalmers University of Technology, Kemivägen 10, 412 96 Gothenburg, Sweden

ARTICLE INFO

Keywords:
Amyloid-β
Endocytosis
Alzheimer's disease
Protein aggregation
Cell surface proteoglycan
Chinese hamster ovary cells

ABSTRACT

Proteoglycans (PGs) have been found in Alzheimer's disease amyloid-β (Aβ) plaques and their glycosaminoglycan chains reportedly influence Aβ aggregation, neurotoxicity and intracellular accumulation in cell and animal models, but their exact pathophysiological role(s) remain unclear. We have studied the cellular uptake of fluorescently labelled Aβ(1–42) and Aβ(1–40) peptides in normal CHO cells (K1) and the mutant cell line (pgsA-745) which lacks all protein-attached heparan and chondroitin sulfate chains. After 24 h of incubation, CHO-K1 accumulates more Aβ(1–42) and Aβ(1–40) compared with CHO-pgsA-745, consistent with the suggested role of PGs in Aβ uptake. However, after short incubation times (≤3 h) there was no difference; moreover, the time evolution of Aβ(1–42) accumulation in CHO-K1 followed an unusual sigmoidal-like trend, indicating a possible involvement of PG-mediated peptide aggregation in Aβ endocytosis. Neither Aβ(1–42) nor Aβ(1–40) could stimulate uptake of a 10 kDa dextran (a general endocytosis marker) suggesting that Aβ-induced upregulation of endocytosis does not occur. CHO-K1 cells contained a higher number of Aβ(1–42)-positive vesicles, but the intensity difference per vesicle was only marginal suggesting that the superior accumulation of Aβ(1–42) stems from a higher number of endocytic events. FRET imaging support that intracellular Aβ(1–42) is aggregated in both cell types. We also report that CHO-pgsA-745 cells perform less endocytosis than CHO-K1 and, albeit this does not explain their difference in Aβ internalisation, we discuss a general method for data compensation. Altogether, this study contributes new insights into the mechanisms of PG-mediated Aβ uptake that may be relevant for our understanding of their role in AD pathology.

1. Introduction

Alzheimer's disease (AD) is the most common form of dementia affecting > 40 million people worldwide [1]. Extracellular amyloid-β (Aβ) plaques [2,3] as well as intracellular neurofibrillary tau tangles [4] are major disease hallmarks, but the molecular pathology of the disease remains unclear. Aβ peptides are cleavage products of the amyloid precursor protein (APP); the proteolytic processing occurs predominantly in acidic vesicular organelles of neurons whereupon the peptides can be secreted or retained [5]. Intraneuronal Aβ build-up is one of the earliest pathological signatures of AD, appearing before the formation of extracellular plaques [6–8]. In order to understand how extracellular and intracellular Aβ pools are inter-related we have herein explored the mechanisms and interactions that contribute to Aβ uptake and accumulation. Aβ peptides, in various forms, enter cultured cells via endocytosis [9–12]. We have shown that uptake of Aβ(1–40) and Aβ(1–42) monomers is independent of clathrin and dynamin, but perturbed by actin depolymerisation and pharmacological inhibitors of macropinocytosis [10]. Because of the common involvement of cell surface proteoglycans in macropinocytosis and their association with AD pathology (see below) we here focus on their role in the internalisation of Aβ(1–42) monomers.

Glycosylated proteins (proteoglycans, PGs) have been implicated in several stages of the Aβ pathogenesis in AD. It is now over 30 years since they were first found to co-deposit with Aβ into senile plaques [13]. More recent data has shown that it is both heparan sulfate-carrying proteoglycans (HSPGs) and chonditrin sulfate-carrying proteoglycans (CSPGs) that are found in plaques [14–16]. Soluble heparan sulfate or chondroitin sulfate glycosaminoglycans (GAGs) have been shown to attenuate Aβ(25–35) neurotoxicity in cultured hippocampal

* Corresponding author.
E-mail address: eline@chalmers.se (E.K. Esbjörner).

https://doi.org/10.1016/j.bbamem.2018.08.010
Received 24 January 2018; Received in revised form 30 July 2018; Accepted 19 August 2018
Available online 23 August 2018
0005-2736/

neurons to comparable extents [17]; a HSPG-deficient CHO cell line was also observed to be resilient to Aβ toxicity [18]. Both GAG types have been reported to catalyse Aβ peptide aggregation [19,20]; this has been suggested to critically depend on the sulfate moieties of the GAG chains [19]. Furthermore, Castillo et al. [21] demonstrated Aβ peptide binding as well as promoted fibrillation with surface-immobilized HSPGs of perlecan type, suggesting that aggregation-promoting reactions can also occur at cellular membranes. This is perhaps particularly interesting in relation to *in vitro* data showing that heparin, a GAG with similar glycosylation pattern as in heparan sulfate, mainly bind to Aβ fibrils [22] and a recent NMR study that revealed close contacts between heparin and one or several histidine residues in Aβ(1–40) fibrils [23], suggesting a role for electrostatic interaction. The amount of HSPGs has been observed to be increased in postmortem human brain tissues from AD patients relative to healthy controls; based on recent studies in transgenic mice these moieties where furthermore proposed to be involved in both Aβ aggregation and its clearance from interstitial fluid [24]. Although apparently less studied, alterations in molecular compositions of cerebral chondroitin sulfate in AD transgenic mice have also been reported [25]. Several studies have pointed to that presence of cell-surface proteoglycans lead to enhanced intracellular accumulation of Aβ, but all have been conducted with long term (24 h) incubation [18,26,27]. We have used Chinese hamster ovary (CHO) cells with normal PG expression (CHO-K1) as well as the engineered PG-deficient CHO-pgsA-745 mutant. Sandwall et al. [18] have characterised the GAG composition of CHO-K1 cells. Their analysis showed that HS and CS are present in equal amounts (46 and 54% respectively); this, in combination with the above-mentioned putative roles of both GAGs in AD and Aβ pathology, prompted us to the CHO-pgsA-745 cell line in our studies. CHO-pgsA-745 are deficient in xylotransferase which catalyses the first sugar transfer in GAG synthesis, and these cells do therefore not produce any GAGs [28] and are thus completely devoid of protein-attached sulphated sugars on their cell surfaces. Our study focuses particularly on the role of protein-attached sulphated sugars (hereafter denoted cell surface PGs) in the cellular uptake of Aβ(1–42), added to cells in the form of soluble monomers. Furthermore, we have treated cells with Aβ for different incubation periods. This has revealed new information on how PG-dependent Aβ uptake evolves with time and thereby provide additional insights into how PGs may mediate intraneuronal Aβ accumulation.

2. Materials & methods

2.1. Reagents

Synthetic Aβ(1–42) (and Aβ(1–40)) peptides, conjugated to the HiLyte Fluor™ (HF) fluorophore HF488 or HF647 at the N-terminus as well as unlabelled variants, were purchased from Anaspec Inc. (Fremont, US). Unless specifically noted, experiments were performed with the HF488-labelled peptides. The peptide purity was > 95% as determined by Anaspec by mass spectrometry and reverse phase HPLC. AlexaFluor488 (AF488)- and AlexaFluor647 (AF647)-labelled 10 kDa dextrans with negative charge were from Molecular Probes and purchased via ThermoFisher Scientific (Gothenburg, Sweden). Cell Tracker Red CMTPX (Invitrogen) was also purchased via ThermoFisher Scientific. The Chinese hamster ovary cell line CHO-K1 (ATCC® CCL-61™) and the proteoglycan-deficient mutant cell line CHO-pgsA-745 (ATCC® CRL2242™) were acquired from ATCC (Wezel, Germany). Cell culture reagents (nutrient mixture F-12 Ham, heat-inactivated fetal bovine serum, trypsin-EDTA 0.05%, and HEPES buffer) were from HyClone (GE Healthcare, South Logan, US) and L-glutamine was from Gibco/Life Technologies and purchased via ThermoFisher Scientific.

2.2. Preparation and handling of Aβ peptides

The lyophilized Aβ peptide powders were dissolved in hexafluoro-2-propanol to disrupt any aggregates [29] and monomerize the peptide. The solutions were vortexed briefly and aliquoted at 4 °C. The solvent in each aliquot was evaporated at 37 °C for 15 min on a heating block followed by 45 min under vacuum using a RVC 2-18 CD Rotational Vacuum concentrator (Martin Christ, Germany). The resulting peptide films were snap frozen in liquid nitrogen and kept at −80 °C until further use. We have previously confirmed that this protocol yields peptide solutions that, when supplied to cells contains soluble, > 85% monomeric, material [10]. To determine the peptide concentration one peptide film was dissolved in 1% ammonium hydroxide (v/v) and the absorption of the dye label was measured on a Cary 4000 UV–Vis Spectrophotometer (Agilent Technologies, Santa Clara, CA, US). Extinction coefficients of 70,000 $M^{-1} cm^{-1}$ at 504 nm and 250,000 $M^{-1} cm^{-1}$ at 649 nm was used for the HF488 and HF647 dye labels, respectively, according to the information provided by the manufacturer. Prior to each experiment one peptide film was dissolved in a small volume 1% ammonium hydroxide (v/v) and diluted with serum-free cell culture medium supplemented with 30 mM HEPES. The concentration of ammonium hydroxide was kept below 0.002% and was matched in all samples to ensure identical treatment of samples. Diluted samples were used immediately in order to avoid unwanted Aβ aggregation.

Aβ(1–42) oligomers were prepared by resuspending HF488-Aβ(1–42) and unlabelled Aβ(1–42) at a ratio of 1:9 in DMSO followed by dilution in ice-cold 20 mM PBS buffer, pH 7.4 to a concentration of 100 μM and incubation at 4 °C under quiescent conditions over night. For analysis, the oligomers were passed through an Amicon Ultra-0.5 100 kDa cut-off filter (Millipore, US).

2.3. Cell culture and sample preparation

CHO-K1 and CHO-pgsA-745 cells were grown in nutrient mixture F-12 Ham supplemented with 10% heat-inactivated fetal bovine serum (FBS) and 2 mM L-glutamine. The cells were detached (trypsin-EDTA 0.05%, 7 min) and passaged twice a week. Cells were plated one day prior to experiments in flat-bottomed 96 well plates (Nunc; 20,000 cells/well) for flow cytometry or two days prior to experiments in glass-bottomed culture dishes (MatTek; 20,000 cells/14 mm dish) for microscopy. All cell samples were washed 1× in serum free medium prior to incubation with the Aβ peptides and/or the 10 kDa dextrans. All incubations were performed in serum free medium supplemented with 30 mM HEPES.

2.4. Flow cytometry

Flow cytometry was used for quantification of cellular uptake. Prior to analysis, the cells were always washed 2× in ice-cold serum free medium, detached by trypsin-EDTA 0.05% for 10 min followed by addition of ice-cold FBS-supplemented cell culture medium to inhibit further proteolytic degradation of the cells. All samples were kept on ice until they were analysed on a Guava EasyCyte 8HT (Millipore, Darmstadt, Germany) that automatically retrieves samples from a 96-well plate. In order to exclude effects due to difference in delay time we used mixed order of analysis, loading only a few samples at a time with the remaining samples kept on ice. Only the central cell cluster on the forward/side scatter (FSC/SSC) dot plot was analysed and for each sample 5000 cells from within the gate were counted. The HF488 and AF488 fluorophores were excited by a 488 nm laser and fluorescence was detected through a 525/30 nm filter. AF647 was excited with a 635 nm laser and detected through a 661/19 nm filter. The mean cellular uptake was estimated as the average fluorescence intensity of all cells gated on the central cluster of the FSC/SSC dot plot. The mean cellular uptake was baseline corrected by subtracting the signal recorded for untreated cells. Each cell treatment was performed in three to five technical replicates (n = 3–5) and repeated on at least two separate occasions (N ≥ 2) unless else is noted. All flow cytometry data

was analysed in InCyte software (Millipore, Darmstadt, Germany) and displayed using Origin software (OriginLab, Northampton, MA, US).

2.5. Confocal microscopy and FRET analysis

Prior to imaging, the cells were washed 1× in serum-free medium to remove extracellular Aβ/dextran and thereafter imaged immediately. In experiments using CellTracker Red CMTPX to stain the cell body, this reagent was added to the cells at a concentration of 1 μM in serum-free medium and allowed to equilibrate for 30 min prior to the washing step. Confocal images were acquired on an inverted Nikon C2+ confocal microscope equipped with a C2-DUVB GaAsP Detector Unit with variable emission bandpass, using an oil-immersion 60 × 1.4 Nikon APO objective and the 488 and/or 640 nm laser lines (Nikon Instruments, Amsterdam, Netherlands). The fluorescence was detected between 500 and 550 nm and 650–700 nm for the green and red channel respectively.

For FRET experiments, cells were incubated with either 500 nM HF488-Aβ(1–42) or 500 nM HF647-Aβ(1–42), or an equimolar mixture of the two (total concentration 1 μM) for 24 h. The samples were then imaged sequentially in green (excitation 488 nm/emission 500–550 nm), red (excitation 640 nm/emission 650–700 nm) and FRET (excitation 488 nm/emission 650–700 nm) channels. The laser power and detector gain for each individual channel was kept constant throughout the experiment. 6–10 images were captured per cell culture dish, with on average 24 cells per image. The experiment was repeated on two separate occasions (N = 2). The images were analysed in ImageJ (NIH, Bethesda, Maryland, US). A mask corresponding to Aβ(1–42) containing intracellular regions was made by applying Gaussian blur followed by background correction of the green and red channels, whereupon the two channels were added. The resulting image was converted to a 32-bit mask by translating all pixels ≥1 to 1 and remaining pixels to NaN. The resulting masked image was compared with the original green and red channels to confirm the correctness of the mask. The single labelled Aβ(1–42) samples were then treated by background correction and conversion to 32-bit images, followed by multiplication with the mask and summation of total image intensity. The extent of bleed-through of HF488 emission into the FRET channel was determined by dividing the intensity in the FRET channel by the intensity in the green channel for the HF488-Aβ(1–42) single-labelled sample; the extent of cross-excitation of HF647 influencing the signal in the FRET channel was calculated by dividing the intensity in the FRET channel by the intensity in the red channel for the HF648-Aβ(1–42) single-labelled sample. The dual-labelled samples were background corrected and masked as described above and thereafter the FRET data were corrected for bleed-through and cross-excitation by subtraction of the green and red channels multiplied by the extent of bleed-though and cross-excitation, respectively. The average intensity of all masked pixels was calculated for each individual image.

2.6. Time of flight secondary ion mass spectrometry (ToF-SIMS) analysis

Time of flight secondary ion mass spectrometry (ToF-SIMS) was used to probe differences in cell surface glycosaminoglycans on the surface of the CHO-K1 and CHO-pgsA-745 cells. 250,000 cells were seeded on 13 mm Thermanox™ cell culture-treated plastic coverslips and allowed to grow for 24 h. The cell culture media was removed and the cells were first washed in PBS supplemented with calcium and magnesium salt, and thereafter gently washed at room temperature for 30 s with ammonium acetate (150 mM) followed by a 10 s wash in milli-Q water, whereafter the samples were air dried for 24 h in a laminar flow hood as described by Brison et al. [30]. ToF-SIMS analysis was then performed using an IONTOF V ToF-SIMS instrument (IONTOF GmbH, Münster, Germany) equipped with a Bi_3^+ cluster ion gun as primary ion source. 3–4 areas of 100 × 100 μm from each cell type were analysed in positive mode. Regions of interest corresponding only the cell membrane was selected and compared. The ion dose density was maintained at 1×10^{11} ions cm^{-2}, i.e. below the static limit (1×10^{13} ions cm^{-2}) to reduce surface damage. Data analysis was performed with Surface Lab software (version 6.7 IONTOF, GmbH, Münster, Germany). The recorded spectra were internally calibrated to signals of [C]+, [CH]+, [CH2]+, [CH3]+, [C5H15PNO4]+ and [C27H45]+.

2.7. Atomic force microscopy (AFM)

Aβ(1–42) oligomers were deposited on freshly cleaved mica and allowed to settle for 5 min before rinsing with filtered milli-Q water, whereafter the samples were dried under a gentle nitrogen stream. The samples were analysed using an NTEGRA Prima setup (NT-MDT Spectrum Instruments, Moscow, Russia) with a gold-coated single crystal silicon cantilever (NT-MDT, NSG01, spring constant of ~5.1 N/m) and a resonance frequency of ~150 kHz. Images were acquired at 512 pixel resolution with 0.5 Hz scan rate.

2.8. Statistics

All flow cytometry data are presented as mean ± standard deviation (SD) of N independent sets of experiments, each with n technical replicates. 5000 cells from within the central cell cluster on the forward/side scatter (FSC/SSC) dot plot was analysed for each replicate. Since the absolute fluorescence intensity recorded on our flow cytometer varies slightly between experiments performed on different days, the presented data has been normalised as stated in the figure texts, typically the normalisation was to the fluorescence signal from CHO-K1 cells incubated with Aβ(1–42) for 24 h. This made it possible to combine and analyse data collected on separate occasions. Means comparison was performed by two-tailed two-sample *t*-tests (alpha level 0.05) using Origin software (OriginLab, Northampton, MA, US).

3. Results

3.1. Cell uptake and intracellular distribution of Aβ(1–42)

We used live cell confocal microscopy imaging as well as flow cytometry to monitor the uptake and intracellular distribution of Hilyte Fluor™ 488 (HF488)-labelled Aβ peptides into Chinese hamster ovary cells with (CHO-K1) and without (CHO-pgsA-745) proteoglycan attached glycosaminoglycans (hereafter denoted as PG-deficient cells). The CHO-pgsA-745 cells are deficient in xylosyl transferase and therefore completely lack the ability to synthesize PG-attached chondroitin and heparan sulfate chains [28], they still, however, express PG core proteins. Our study is focused on Aβ(1–42), the most toxic [31] and aggregation prone [32] Aβ variant, but we also present comparative data for Aβ(1–40) in the supporting information. Throughout this study the cells were treated with Aβ solutions that, at time of application to the cells, were mainly monomeric (> 85%, according to SDS-PAGE analysis [10]). The HF488-Aβ(1–42) (hereafter denoted only Aβ(1–42)) peptide solutions were prepared as described previously [10] and in Section 2.2.

In a first set of experiments, we exposed the two cell types to 1 μM solutions of Aβ(1–42) for 24 h followed by confocal fluorescence microscopy analysis where Z-stacks were recorded in order to determine the intracellular accumulation and distribution of the peptide. The images in Fig. 1A–B show that the Aβ(1–42) peptides (green) were localised within the cell body (counterstained with Cell Tracker Red CMTPX) and distributed to discrete puncta. Furthermore, a time-lapse movie showing the uptake of Aβ(1–42) in CHO-K1 cells (Supporting Video S1) suggests that the cells preferentially internalize Aβ(1–42) at the actin polymerization-rich leading edge and into mobile vesicles, consistent with endocytosis as previously reported by us and others [9–12]. Similar intracellular distribution patterns were observed for

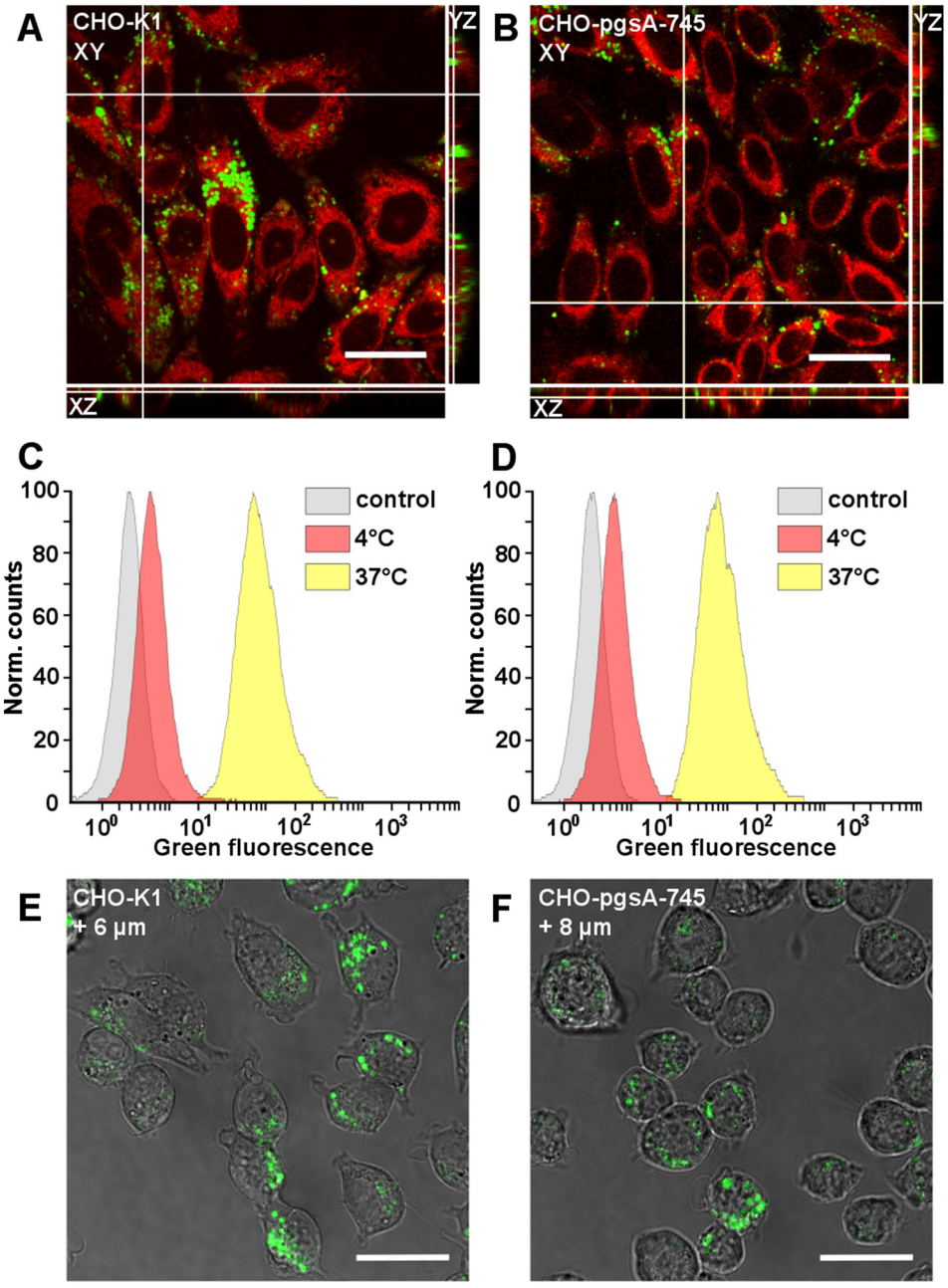

Fig. 1. Cell uptake and distribution of Aβ(1–42) in CHO-K1 and PG-deficient CHO-pgsA-745 cells. (A–B) Confocal fluorescence microscopy images of Aβ(1–42) (green) in live CHO-K1 (A) and CHO-pgsA-745 (B) cells after 24 h incubation with an initially monomeric peptide solution. The images show one confocal plane (XY) from within the cells with orthogonal XZ and YZ projections. The cell bodies were counterstained with Cell Tracker Red CMTPX (1 µM) 30 min prior to imaging. The scale bars are 20 µm. (C,D) Flow cytometry histograms showing the green fluorescence in CHO-K1 (C) and CHO-pgsA-745 (D) cells treated with HF488-Aβ(1–42) for 3 h at normal conditions (37 °C) or at 4 °C to block endocytosis. (E,F) Confocal fluorescence microscopy images of 2× washed and trypsinized CHO-K1 (E) and CHO-pgsA-745 (F) cells that had been treated with Aβ(1–42) for 24 h. The distance above the cover slip of the confocal plane is indicated; full z-stacks are shown in Supplementary Fig. S2. The Aβ(1–42) concentration in all experiments was 1 µM. The scale bars are 20 µm.

Aβ(1–40) (Supplementary Fig. S1). The cell uptake path was further analysed by comparing peptide accumulation (measured by flow cytometry) into cells that had been incubated with Aβ(1–42) for 3 h at 4 °C and 37 °C respectively; the former condition inhibits all forms of endocytic internalisation [33]. Representative flow cytometry histograms are shown in Fig. 1C–D and reveal that cells that were kept at 37 °C had approximately one order of magnitude higher average fluorescence intensity compared with cells incubated at 4 °C; there was no difference between the CHO-K1 and CHO-pgsA-745 cell types. Although Aβ peptides appear not to accumulate extensively at the plasma membrane prior to internalisation (Supporting Video S1, [10,11]) we performed an additional control experiment in which cells were washed and trypsinized with the same protocol as used for flow cytometry, but thereafter instead imaged by confocal microscopy (Fig. 1E–F; the full Z-stacks are shown in Supplementary Fig. S2). No significant cell-surface associated fluorescence was observed, strongly suggesting that the cellular fluorescence intensities that we record by flow cytometry can be regarded to stem from intracellular Aβ(1–42) only.

3.2. Comparison of endocytic capacity and cell surface composition in CHO-K1 and CHO-pgsA-745 cells

Proteoglycans (PGs) have been implicated in several types of endocytosis, including macropinocytosis, flotillin-dependent, and dynamin-dependent endocytosis [34–36]. Removal of all PG-attached heparan and chondroitin sulfate GAGs from the cell surface, as is the case for the CHO-pgsA-745 cells, could therefore be expected to perturb the intrinsic endocytic capacity of the cell and reduce the number of endocytic events; a circumstance that has, to the best of our knowledge, not been addressed despite the common use of these cell lines in uptake studies. We used a small (10 kDa) fluorescent dextran tagged with AlexaFluor-488 (AF488) to estimate the relative endocytic activity of the CHO-K1 and CHO-pgsA-745 cells. Dextran is a generic fluid-phase endocytosis marker that has been reported to internalize via both macropinocytic and micropinocytic pathways, including clathrin-mediated endocytosis [37,38]. Cells were first treated with dextran for 24 h and imaged by confocal fluorescence microscopy to confirm

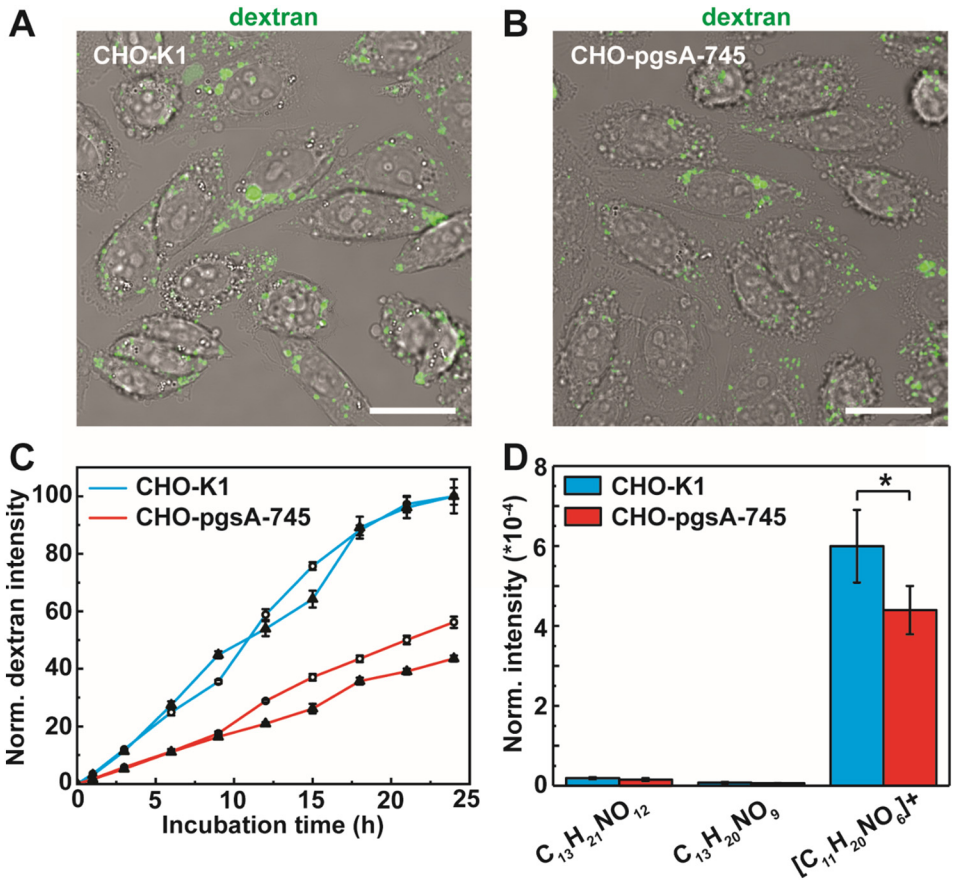

Fig. 2. Endocytic capacity and cell surface composition of CHO-K1 and CHO-pgsA-745 cells. (A–B) Confocal fluorescence microscopy images of CHO-K1 (A) and CHO-pgsA-745 (B) cells incubated with 125 μg/ml AF488-labelled dextran 10 kDa (green) for 24 h. The images show an overlay of the green channel and the transmitted image. Each image has been adjusted individually to best represent the intracellular pattern and the intensities are thus not comparable. The scale bars are 20 μm. (C) Cellular uptake of 125 μg/ml AF488-labelled 10 kDa dextran as function of time measured by flow cytometry. Two separate sets of experiments are shown (closed triangles and open circles respectively, n = 5). All data have been normalised to the cellular intensity in CHO-K1 cells after 24 h of incubation. The ratio of dextran uptake, and hence endocytic activity ratio (see text) between CHO-K1 and CHO-pgsA-745 was 1.97 and 2.37 in the two respective experiments. (D) ToF-SIMS average ion intensities of peaks attributed to cell surface heparan sulfate and chondroitin sulfate from CHO-K1 and CHO-pgsA-745 cells showing a reduction of peak intensities in the latter. Star over bars indicate statistically significant difference (two-sample *t*-test; $p < 0.05$; n = 3).

punctuate cytoplasmic staining consistent with endocytosis (Fig. 2A–B). Cells were thereafter analysed for dextran uptake by flow cytometry every third hour for up to 24 h to determine the relative accumulation in the two cell types (Fig. 2C). The dextran uptake is clearly higher in CHO-K1 than in CHO-pgsA-745 throughout the assayed time interval, confirming the idea that PG-GAG deficient cells perform less endocytosis. Moreover, we find that dextran accumulation increases linearly with time in both cell types and thus without signs of saturation. We used linear regression to fit the data from each separate set of experiments and thereafter derived an endocytic activity ratio ($E_{CHO\text{-}K1}/E_{CHO\text{-}pgsA\text{-}745}$) from the quotient of the slopes of the fitted lines. This analysis shows that the dextran uptake is ~2 times higher in CHO-K1 compared CHO-pgsA-745 cells under our experimental conditions. One rational interpretation of this result is that approximately 50% of the basal endocytosis in CHO-K1 is dependent on functional PGs. We repeated the experiments also with an AF647-labelled 10 kDa dextran to exclude the possibility that the dye label itself influences dextran uptake. The results were near identical (Supplementary Fig. S3).

We have previously compared the two CHO cell types with respect to their zeta potential and electrophoretic mobility and found insignificant differences in cell surface charge, despite the removal of all PG-associated GAGs in CHO-pgsA-745 cells [39]. Here we performed further comparative analysis of the two cell types using time of flight secondary ion mass spectrometry (ToF-SIMS). ToF-SIMS is a surface sensitive technique that can be used to probe the cell membrane for molecular changes [40,41] and is often used to track changes in lipids, glycans and saccharides [42–44]. Here ToF-SIMS was used to track heparan sulfate and chondroitin sulfate on the plasma membrane of the two cell types. There was a pronounced difference between the CHO-K1 cells and the CHO-pgsA-745 cells in a number of peaks that can be attributed to heparan sulfate and chondroitin sulfate, e.g. C11H20NO6 at *m/z* 262.1, C13H20NO9 at *m/z* 334.1 and C13H21NO12 at *m/z* 383.3, as can be seen in Supplementary Fig. S4. The average intensities from these peaks are plotted in Fig. 2D, demonstrating diminished intensities for the CHO-pgsA-745 cells consistent with their lack of PG-associated GAGs.

3.3. Flow cytometry analysis of the accumulation of Aβ peptides in CHO-K1 and CHO-pgsA-745 cells

We used flow cytometry to determine the relative accumulation of Aβ peptides in the two cell types 3 and 24 h after addition of monomeric peptide solutions to the cells. Fig. 3A shows the average cellular fluorescence intensity of the HF488 label for cells incubated with Aβ(1–42). The data, which have been obtained from four independent experiments performed on different batches of cells and peptides, is normalised so that the mean cellular intensity for CHO-K1 cells treated with Aβ(1–42) for 24 h is set to a value of 100 a.u. in order to account for intensity variations in between experimental days (mainly due to instrument performance, see Section 2.8). After 24 h, the average cellular intensity is markedly higher (~13 times) for the CHO-K1 compared with the CHO-pgsA-745 cells. Corresponding data for Aβ(1–40) are presented in Supplementary Fig. S5 and show ~7 times higher average cellular intensity in the CHO-K1 cells. These results are well in line with a previous report by Kanekiyo et al. [27]. However, we found that with a much shorter incubation time (3 h) the result was significantly different; although the CHO-K1 cells still accumulate more Aβ(1–42) than CHO-pgsA-745, the difference after 3 h is only 2-fold. Considering our observation of an inherent difference in dextran uptake between the two cell types (Fig. 2C) which can be interpreted as a reduction in endocytosis for the PG-GAG deficient CHO-pgsA-745 cells, we argue that it can be justified to correct cell uptake data for this difference, particularly under conditions where the uptake differences in CHO-K1 and CHO-pgsA-745 are small. We plotted such corrected

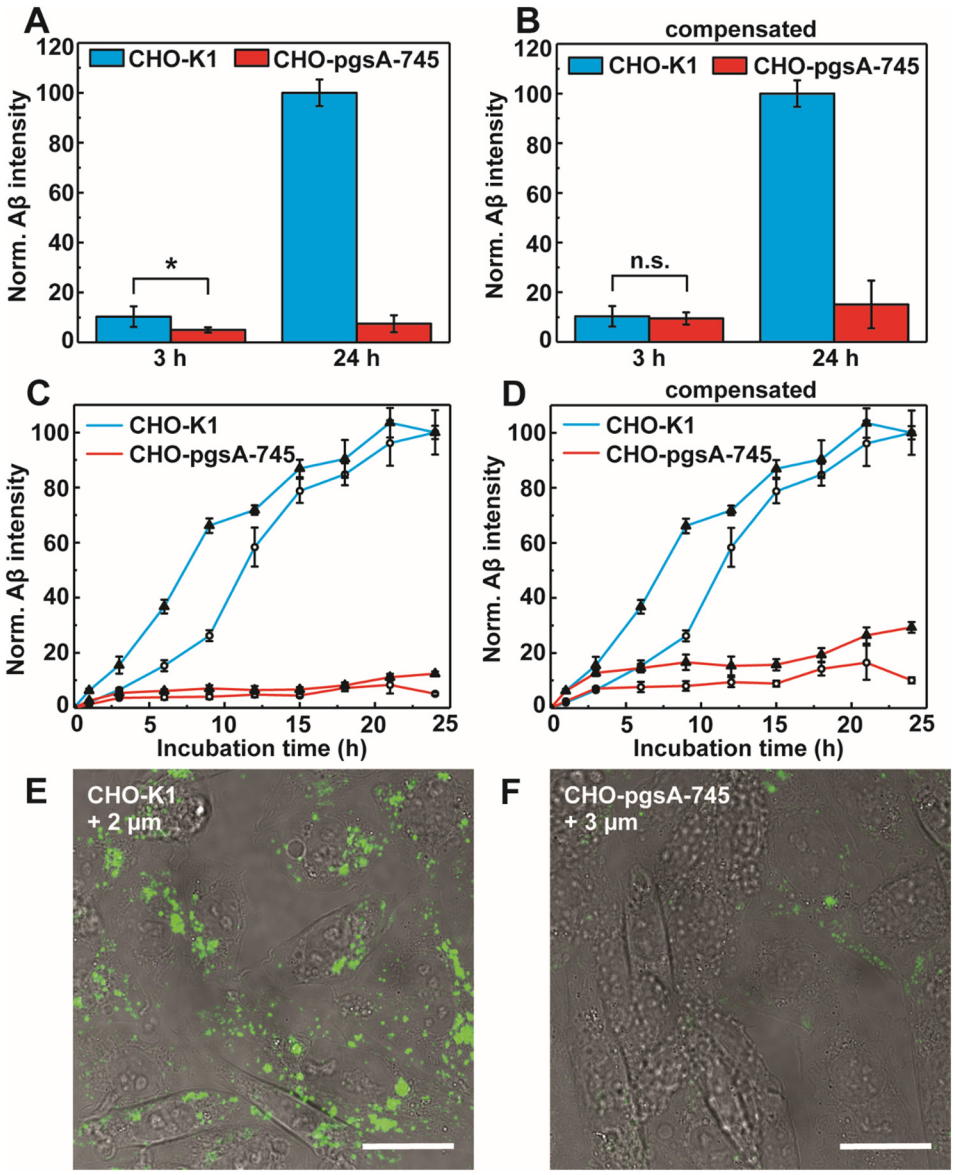

Fig. 3. Cellular uptake of Aβ(1–42) in CHO-K1 and PG-deficient CHO-pgsA-745 cells as function of time. (A) Relative quantification of the cellular uptake of 1 µM Aβ(1–42) in CHO-K1 and CHO-pgsA-745 cells after 3 h and 24 h measured by flow cytometry. All data have been normalised to the cellular intensity of Aβ(1–42) in CHO-K1 cells after 24 h. The stars above bars indicate statistically significant mean difference (two-sample *t*-test on four individual sets of data as well on the combined data, p-values: 8E − 6 to 0.007, N = 4, n = 3–5). (B) Relative cellular uptake of Aβ(1–42) after compensation for cell line dependent differences in endocytic activity/dextran uptake (see Fig. 2C and text). (C) Cellular uptake of Aβ(1–42) as function of time measured by flow cytometry. Data from two independent experiments are shown (closed triangles and open circles respectively, n = 5). The peptide concentration was 1 µM. All data have been normalised to the cellular intensity of Aβ(1–42) in CHO-K1 cells after 24 h of incubation. (D) Relative cellular uptake of Aβ(1–42) after compensation for cell line dependent differences in endocytic activity/dextran uptake (see Fig. 2C and text) (E–F) Intensity-matched confocal fluorescence microscopy images overlaid onto the transmitted image of Aβ(1–42) in CHO-K1 (E) and CHO-pgsA-745 (F) cells after 24 h of incubation. The distance above the cover slip of the confocal plane is indicated in the image. The scale bars are 20 µm.

data in Fig. 3B and show that upon compensation for the differences in endocytic activity between the cell lines the uptake levels of Aβ(1–42) after 3 h become indistinguishable (two-sample *t*-test, p-value 0.45). Taken together, these data support the idea that PGs mediate Aβ uptake, but our results also show that it takes at least 3 h of continuous exposure to Aβ(1–42), added at time zero as a mainly monomeric solution, before the PG-presenting CHO-K1 cells begin to accumulate significantly more peptide than the proteoglycan-deficient CHO-pgsA-745 cells. At 3 h of incubation, the uptake into CHO-K1 and CHO-pgsA-745 merely appear to occur in proportion to each cell type's endocytic activity.

We also compared the relative accumulation of Aβ(1–40) and Aβ(1–42) in CHO-K1 as well as in CHO-pgsA-745 after 24 h of incubation. We found that CHO-K1 accumulate ~3 times more Aβ(1–42) than Aβ(1–40) whereas for CHO-pgsA-745 the relation is ~2-fold (Supplementary Fig. S6). Both results are in agreement with what we have previously reported using human neuroblastoma cells [10]. The greater difference between cell lines for Aβ(1–42) compared with Aβ(1–40) could suggest that Aβ(1–42) uptake is more highly dependent on PGs than the uptake of Aβ(1–40).

Next we explored how Aβ(1–42) accumulation in the CHO-K1 and CHO-pgsA-745 cells developed over time during continuous incubation to assay time points in between 3 and 24 h. Fig. 3C shows the change in mean intracellular intensity (measured by flow cytometry) of Aβ(1–42) as function of time from two independent sets of experiments. Fig. 3D shows corresponding curves after correction for cell type differences in dextran uptake (endocytic rate) as described above. Although the curves are slightly different, they clearly show a continuous, but non-linear, increase in the amount of intracellular Aβ(1–42) over time in the CHO-K1 cells. The shapes of the curves suggest a sigmoidal-type time evolution, resembling the kinetic behavior for Aβ(1–42)'s in vitro aggregation [45,46]. This is clearly distinct from the linear uptake behavior of dextran and suggests that in PG-presenting cells, Aβ(1–42) accumulation has a more complex time-dependent behavior. Corresponding data for Aβ(1–40) (Supplementary Fig. S7) instead show a steady rise in uptake with saturation after 10–15 h; the two peptide variants interestingly appear to behave differently. One possible interpretation of our results is that PG-dependent Aβ(1–42) uptake could be catalyzed by aggregation of the Aβ(1–42) peptide; such reactions could potentially occur locally at the cell surface [47]. The uptake of Aβ(1–42) (and Aβ(1–40), Supplementary Fig. S7) into CHO-pgsA-745 cells is, on the other hand, consistently low throughout the 24 h experiment and does not appear to have any sigmoidal-shaped change. We collected cell media from the experiments presented in Fig. 3C and

analysed their Aβ(1–42) content using SDS-PAGE. We observed no oligomeric species on the gel (Supplementary Fig. S8). Further, the Aβ(1–42) monomer bands showed no change in intensity with time, suggesting that amyloid formation in bulk did not occur; a finding that is consistent with the low Aβ(1–42) concentrations used.

The results from flow cytometry of superior Aβ(1–42) uptake in CHO-K1 cells after 24 h of incubation is additionally supported by the confocal fluorescence microscopy images shown in Fig. 3E–F, which were recorded with identical microscope settings and on the same day to allow for direct comparison of their intensities.

3.4. PG-mediated Aβ(1–42) uptake does not result from stimulation of endocytosis

To rationalize the finding that PG-mediated Aβ(1–42) uptake increases in a sigmoidal fashion with time we next considered two possible explanations; either the peptide aggregates in the vicinity of the cell surface (which would be a time-dependent process and consistent with a sigmoidal shape due to the nucleation-dependent behavior of amyloid formation) or the PG-displaying CHO-K1 cells increase their endocytic activity in response to Aβ(1–42) exposure. The latter behaviour has been observed before with the cell-penetrating peptide Tat [48] and in our own studies of different analogs of the Antennapedia homeodomain peptide penetratin [49]. To test this idea, we first measured the endocytic activity of the CHO-K1 and the CHO-pgsA-745 cells after 24 h of pre-treatment with 1 μM Aβ(1–42). At this time point the cells were washed (2×) in serum free media and immediately incubated with AF647-labelled 10 kDa dextran for an additional 3 h. Dextran uptake was then analysed by flow cytometry and the results are shown in Fig. 4A (corresponding results for Aβ(1–40) are shown in Supplementary Fig. S9A). Both figures show identical dextran uptake in untreated and Aβ pre-treated cells. Moreover, the endocytic activity of the CHO-K1 cells remain twice as high as that of the CHO-pgsA-745 cells consistent with the data in Fig. 2C. We thereafter tested if Aβ(1–42) could transiently stimulate endocytic events that internalize dextran by co-incubating the two molecules with cells for 24 h, but neither this resulted in any change in dextran uptake relative to control (Fig. 4B). Similar results were obtained for Aβ(1–40) (Supplementary Fig. S9B). Altogether these experiments refute the idea that Aβ(1–42) and Aβ(1–40) would be capable of stimulating endocytosis to enhance their uptake. On the other hand, we made the interesting observation that the uptake of Aβ(1–42) and Aβ(1–40) is, in fact, slightly to moderately reduced by co-incubation with dextran (Supplementary Fig. S10). Here it should be noted that the 125 μg/ml dextran corresponds to a molar concentration of 12.5 μM; dextran is thus present in vast excess. Nevertheless, it appears as if the two molecules are, at least partly, competing for the same cell surface binding partners and uptake paths.

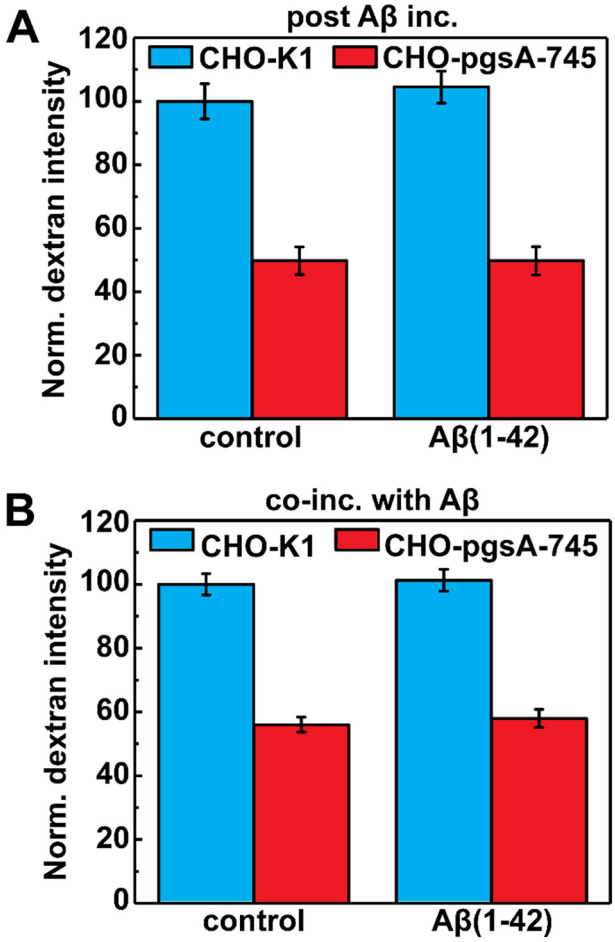

Fig. 4. Aβ(1–42) treatment does not alter the endocytic activity in the CHO-K1 and CHO-pgsA-745 cells. (A) Cellular uptake of AF647-labelled 10 kDa dextran after 24 h pre-treatment with 1 μM Aβ(1–42). After 24 h, the cells were treated with 125 μg/ml dextran for 3 h followed by flow cytometry analysis. The minor differences in mean dextran intensity between control and Aβ(1–42) pre-treated cells are not significant (two-sample *t*-test; p-values of 0.11 and 1.00 were obtained for CHO-K1 and CHO-pgsA-745 respectively, N = 2, n = 4). (B) Cellular uptake of AF647-labelled 10 kDa dextran after 24 h of co-incubation with 1 μM HF488-labelled Aβ(1–42). The minor differences in mean dextran intensity between control and Aβ(1–42) co-incubated cells are not significant (two-sample t-test; p-values of 0.50 and 0.15 were obtained for CHO-K1 and CHO-pgsA-745 respectively, N = 2, n = 4). The data in (A) and (B) have been normalised to the cellular intensity of dextran in CHO-K1 control cells (which were not pre-incubated/co-incubated with Aβ(1–42)).

3.5. Cell uptake and accumulation of pre-formed Aβ(1–42) soluble oligomers

We prepared small soluble Aβ(1–42) oligomers by resuspension in DMSO followed by dilution in ice-cold buffer and incubation over night at 4 °C as described in Materials & Methods and in previous work [50,51]. The oligomers were analysed by AFM (Fig. 5A) demonstrating the formation of small (< 10 nm in height) round oligomers. We then analysed the oligomer content of the solutions by passing them through a 100 kDa cut off filter followed by analysis of the retentate and filtrate by SDS-PAGE and AFM (Supplementary Fig. S11). This confirmed that the oligomers were formed in high yield consistent with our previous work where we determined the yield for the formation of similar unlabelled oligomers to ~90% [51]. We added the pre-formed and fluorescently labelled oligomers to CHO-K1 and CHO-pgsA-745 cells and quantified their uptake after 3 and 24 h using flow cytometry (Fig. 5B–D). The results show very little accumulation of the Aβ(1–42) oligomers after 3 h, the low signal is in part an effect of the 10% labelling ratio. After 24 h, the accumulation of the Aβ(1–42) oligomers is ~13 times higher in CHO-K1 compared with CHO-pgsA-745; thus the result is highly similar to what was observed when cells were treated with monomers.

3.6. Fluorescence resonance energy transfer (FRET) imaging reveal the formation of intracellular Aβ(1–42) aggregates following uptake

In order to test the idea that the enhanced cellular uptake of Aβ(1–42) with time that we observe in the PG-displaying CHO-K1 cells (Fig. 3C–D) results from local peptide aggregation at the cell surface we attempted to image cells incubated with equimolar concentrations of HF488- and HF647-labelled Aβ(1–42) by stimulated emission fluorescence resonance energy transfer (FRET). This approach is based on the reasonable assumption that peptide aggregates will incorporate monomers with both labels and thereby exhibit FRET as demonstrated by *in vitro* experiments [52,53] as well as in the vicinity of live cell

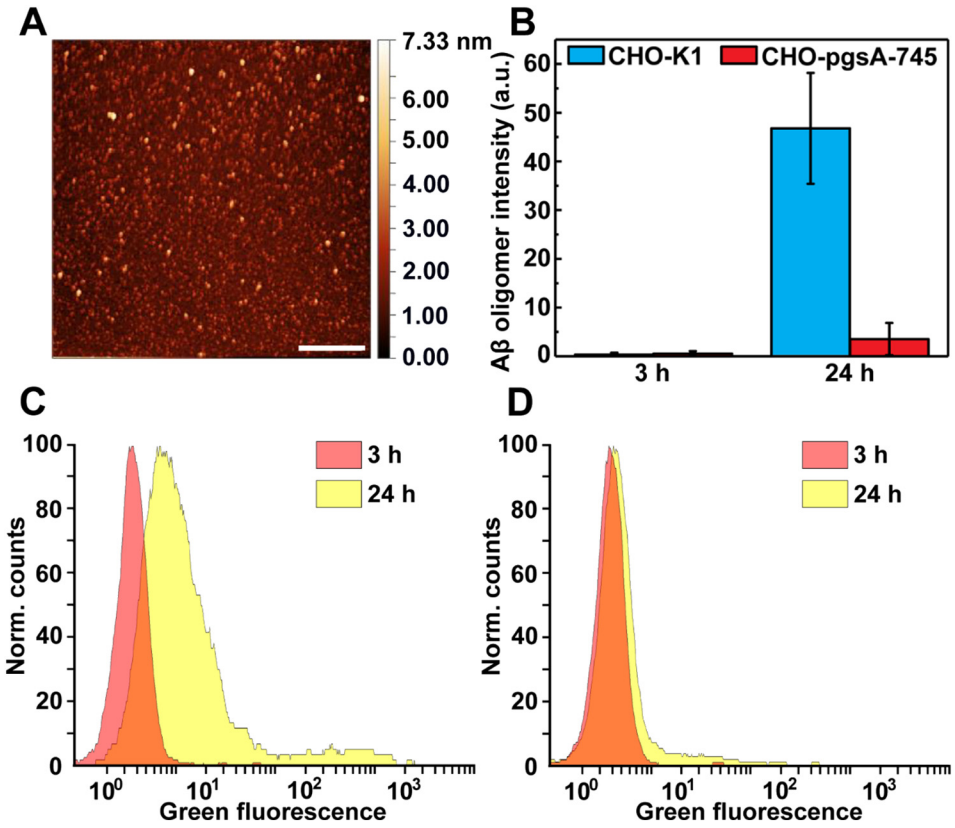

Fig. 5. Cellular uptake of pre-formed Aβ(1–42) oligomers. (A) AFM image of oligomers deposited onto mica showing round morphologies. The scale bar is 1 μm. (B) Cellular uptake of pre-formed Aβ(1–42) oligomers after 3 h and 24 h of incubation measured by flow cytometry (n = 3–4, N = 1 for 3 h timepoint and n = 3, N = 1 for 24 h timepoint). (C–D) Flow cytometry histograms for CHO-K1 (C) and CHO-pgsA-745 (D) cells corresponding to the bar diagram data shown in (B).

membranes [47]. However, we could not observe any peptide accumulation at the cell surface prior to uptake (Fig. 1A–B, Supporting Video S1), consistent with our previous studies in SH-SY5Y cells [10,11]; we presume this is due to that endocytosis is a rapid event. Additional experiments were therefore performed at 4 °C, a temperature that blocks endocytosis [33] whilst retaining the cell membrane intact. Under these conditions, we could detect accumulation of large Aβ(1–42) aggregates/particulates at the cellular membrane (Supplementary Fig. S12) but when the cells were transferred back to 37 °C these were not observed to internalize.

We also probed the accumulation of FRET positive Aβ(1–42) species inside cells by confocal imaging after 24 h of incubation at 37 °C. The acquired data (Fig. 6A–B) were corrected for bleed-through and cross-excitation as described in Section 2.5. It is clear from these images that Aβ(1–42) (regardless of label) accumulates to intracellular puncta in the two cell types. However, the number of bright (above threshold, see Section 2.5) puncta is significantly higher in CHO-K1 compared with CHO-pgsA-745 cells (Fig. 6C). This is consistent with our finding that CHO-K1 accumulate more Aβ(1–42), but also provide additional information about the distribution. We also compared the average pixel intensity in each channel and found that although it is consistently ~1.2 times higher for CHO-K1 compared with the CHO-pgsA-745 cells, the levels are comparable (Fig. 6D). Thus, the higher accumulation of Aβ(1–42) in CHO-K1 appear to result from a greater number of intracellular Aβ(1–42) positive vesicles rather than more Aβ(1–42) per vesicle. Lastly, we analysed the FRET from intracellular Aβ(1–42). The right-most images in Fig. 6A–B indicate that the degree of FRET in the CHO-K1 and CHO-pgsA-745 cells is similar; this conclusion is further corroborated by the similarity in pixel intensity in the FRET channel following normalisation to the intensity in the green (donor) channel (Fig. 6E).

4. Discussion

In this study, we use flow cytometry and live cell confocal fluorescence microscopy to study how the cellular uptake and accumulation of Aβ(1–42) depends on the presence of protein-attached glycosaminoglycans (proteoglycans (PGs)) on the surface of the cells. By comparing cellular accumulation in CHO cells expressing normal HSPGs and CSPGs to CHO cells that lack protein-attached GAG chains (here denoted as PG-deficient although the cells do express the basal proteins to which GAGs are normally attached), we confirm previously published results that cell surface PGs greatly enhance Aβ(1–42) accumulation after 24 h of incubation [18,26,27]. We also, importantly, extend these observations by demonstrating a curious time dependence in the PG-dependent accumulation of Aβ(1–42) uptake, the possible origins of which will be further discussed below. We furthermore demonstrate that Aβ(1–42) uptake occurs without endocytosis stimulation (upregulation), a phenomenon that we have observed for other peptides that are dependent on PGs for their uptake [49]. We find that in PG-presenting cells, Aβ(1–42) is accumulated to a greater number of brightly stained endolysosomal compartments compared with in the PG-deficient cells, which could indicate a larger number of endocytic events. There appear, however, to be no difference in the aggregation of Aβ(1–42) within these intracellular puncta as co-incubation of cells with HF488 and HF647-labelled Aβ(1–42) monomers unconditionally lead to intracellular FRET, extending previous work where we demonstrated such aggregation in PG-presenting neuroblastoma cells using FLIM [11]. The FRET efficiency was independent of the cell's PG-presentation suggesting that the aggregation state of intracellular accumulated Aβ(1–42) is independent of uptake path. Our work extends present knowledge on the role of PGs in Aβ peptide uptake and accumulation and thereby contributes to the complex picture of the molecular pathology of AD.

The main finding of our study is that whereas the cellular uptake of Aβ(1–42) (and Aβ(1–40)) peptides is significantly enhanced in PG-

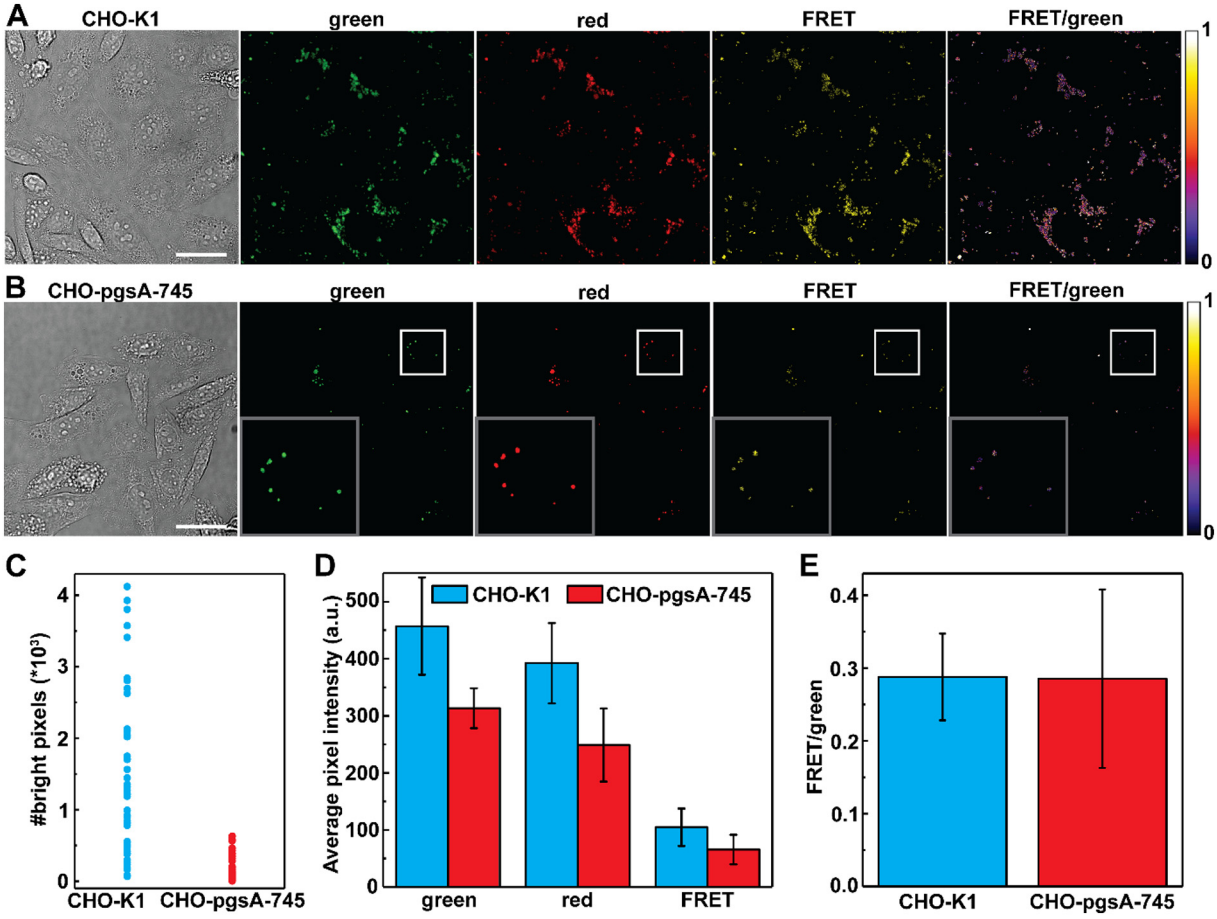

Fig. 6. Confocal microscopy and FRET imaging of intracellular Aβ(1–42). (A–B) Images of CHO-K1 (A) and CHO-pgsA-745 (B) cells incubated with a mixture of 500 nM HF488-Aβ(1–42) (green) and 500 nM HF647-Aβ(1–42) (red) for 24 h. Each image has been processed individually for visualisation purposes, intensities are thus not comparable. Data shown in panels C-E, including FRET calculations, were retrieved from the original, intensity-matched images as described in Section 2.5. The inserts in (B) correspond to a zoom in of the region in the white box. All scale bars are 20 μm. (C) Average number of bright pixels per cell. A total of 48 individual images recorded on two separate occasions, and from in total 6 different cell culture dishes, were included in the analysis for each cell line. Each image contained on average 24 cells. (D) Average pixel intensity in the green, red and FRET channel (± SD). 10 images per treatment were included in the analysis. (E) Average pixel intensity in the FRET image after normalisation with the intensity in the green channel (± SD). 16 images per treatment, recorded on two separate occasions were included in the analysis.

presenting cells upon prolonged (24 h) incubation it is only marginally PG-dependent at short (up to 3 h) incubation time. We note that the intracellular accumulation of Aβ(1–42) with time follows a sigmoidal trend that resembles that of amyloid formation; such trends were not observed for the uptake of the endocytosis marker dextran, nor have we made such observations for the non-aggregating cell-penetrating peptide penetratin [39]; the trend is thus not related to any intrinsic endocytic behaviour of the CHO-K1 cell line. It could be hypothesized that the enhancement in cell uptake with time is a result of Aβ(1–42) aggregation, possibly induced by cell surface localised PG-mediated interactions as SDS-PAGE analysis of cell supernatants suggest that no stable oligomers or fibrils are formed in bulk during the time course of the experiment (Supplementary Fig. S8). Further indirect support of this idea is our finding that the less aggregation prone peptide Aβ(1–40) [32] does not display a sigmoidal trend, at least not in the assayed time interval. As mentioned in the introduction, it has been shown that immobilized GAGs can induce Aβ peptide fibrillation [21], but also oligomerisation [54], and that fibrillar Aβ(1–40) had higher affinity for heparin compared with the non-fibrillar peptide [22]. Although these studies have mainly been performed with HS or HS mimics, it is likely that cell surface immobilized CS would also promote Aβ aggregation as this phenomenon is observed in bulk [19,20]. A recent cell report showed that Aβ(1–42) aggregates appeared locally at the plasma membrane of neurons prior to internalisation [47]. We also observed occasional accumulation of aggregates at the plasma membrane if cells were maintained at 4 °C (Supplementary Fig. S12), but since these occurred in both CHO-K1 and CHO-pgsA-745 cells and were not internalised when cells were brought back to 37 °C it is difficult to judge their relevance. In an additional attempt to test the hypothesis that Aβ(1–42) is taken up more effectively with time due to oligomer formation, we also added small soluble pre-formed oligomers to the cells with the idea that these might be better internalised in CHO-K1 than CHO-pgsA-745 cells even without a lag time. This was, however, not observed; oligomers of the type we produced behave very similar to the monomer. Although this could mean that PG-dependent Aβ(1–42) cell uptake is not dependent on oligomerisation, an alternative explanation is that our pre-formed oligomer have an in-appropriate configuration; a well-known complication in this field [55]. For example, we know from previous work that the type of oligomers used herein is lower in β-sheet content than corresponding fibrils [51]. Since it has been shown that Aβ fibrils have higher affinity for HS than other Aβ types [22] one may speculate that the oligomers we produced simply do not possess optimal spatial arrangement of their β-strands (and histidine residues [23]) to interact with cell surface PGs and that they must therefore dissociate or structurally rearrange (slow processes) prior to cell uptake.

Peptide-induced clustering of cell surface PGs has been reported to stimulate macropinocytosis and thereby increase cellular uptake [49,56]. An alternative explanation to the time evolution we observe

for Aβ(1–42) is that the peptide, with time, cluster PGs and thereby stimulate cellular endocytosis. It is, however, clear from our results that Aβ(1–40) and Aβ(1–42) are unable to induce such effects. Their uptake is thus clearly mechanistically distinct to that of common cell-penetrating peptides, including Tat [48] and penetratin [49] despite that pathway analysis suggest similar involvement of macropinocytosis, or macropinocytosis-like mechanisms in both cases [10,48]. This may be due to that Aβ primarily appear to interact with sulphated sugars via histidine residues whereas many cell-penetrating peptides possess a high number of arginines with capacity of forming very strong bidentate bonds.

We report that one significant reason for the lesser Aβ(1–42) accumulation in PG-deficient CHO-pgsA-745 cells compared with CHO-K1 is that they contain fewer brightly fluorescent Aβ(1–42) positive endolysosomal vesicles; their average intensity per vesicle is, however, only marginally higher in CHO-K1. Although it is not entirely clear how internal endosomes form and mature, it appears that endosome membranes and volume are primarily derived from endocytic vesicles [57] suggesting that a greater number of internal endosomes, as is the case with Aβ(1–42) in CHO-K1, result from a greater number of endocytic events.

CHO-K1 internalize twice the concentration of dextran compared with CHO-pgsA-745 under identical experimental conditions. One very reasonable interpretation of this result is that 50% of the endocytic events in CHO-K1 are dependent of PGs and thus absent in CHO-pgsA-745. It is interesting to note that previous results from our lab on the PG-dependent uptake of penetratin [39] as well as studies of the antisecretory peptide AF-16 [58] actually produce no more than a 2-fold differences in uptake between CHO-K1 and CHO-pgsA-745 cells, suggesting that these peptides use PGs for their uptake, but not to any greater extent than other receptors; this would have been apparent had the results been compensated for the intrinsic differences in endocytic activity between the cell lines, as we propose in this paper. Furthermore, this 2-fold ratio agrees conspicuously well with the Aβ uptake results after 3 h; at this time point the uptake in CHO-K1 is twice as high as in CHO-pgsA-745. We therefore propose that Aβ monomers display no or little preference for PGs because at short incubation times, the added Aβ(1–42) internalize exactly in proportion to the cells basal PG-dependent and PG-independent endocytosis.

In conclusion, PGs of both heparan sulfate and chondroitin sulfate type are present at many important stages of Aβ pathology, but their exact roles and the effect of Aβ-PG interactions are not clear. Our work provides several new pieces of information on how PGs mediate the endocytic uptake of Aβ(1–42). We show that PG-mediated uptake of Aβ(1–42), applied as a monomer solution, increases with time in a sigmoidal fashion and that uptake differences (in excess of what would be expected based on the intrinsic endocytic rate in PG-displaying and PG-deficient cells) take > 3 h to develop. We discuss our result in term of local PG-induced peptide aggregation at the cell surface, and hypothesize that this is driving the very efficient cell uptake that we observe in PG-displaying CHO-K1 cells. We also note that Aβ(1–42) uptake occur without concomitant endocytosis stimulation and that PG-mediated intracellular accumulation of Aβ(1–42) results in a larger number of endolysosomal vesicles which in turn could be consistent with a higher toxic burden [59]. Our findings therefore points to that further explorations into the exact nature of Aβ-PG interactions at the cell surface, including detailed dissection of the putative relevance of different oligomerization states, are warranted and potentially beneficial as targets for future AD therapies.

Supplementary data to this article can be found online at https://doi.org/10.1016/j.bbamem.2018.08.010.

Transparency document

The Transparency document associated with this article can be found, in online version.

Acknowledgements

This work was supported by grants to E.E. from the Wenner-Gren Foundations, the Swedish Research Council-funded Linneaeus centre SUPRA (Grant No. 2016-03902), the Swedish Innovation Agency (Grant No. 2011-03488), the Linnaeus Centre SUPRA, the Magnus Bergvall Foundations, and the IngaBritt and Arne Lundberg foundations.

References

[1] M. Prince, A. Comas-Herrera, M. Knapp, M. Guerchet, M. Karagiannidou, World Alzheimer Report 2016, Alzheimer's Disease International, 2016.
[2] G.G. Glenner, C.W. Wong, Alzheimer's disease: initial report of the purification and characterization of a novel cerebrovascular amyloid protein, Biochem. Biophys. Res. Commun. 120 (1984) 885–890.
[3] C.L. Masters, G. Simms, N.A. Weinman, G. Multhaup, B.L. McDonald, K. Beyreuther, Amyloid plaque core protein in Alzheimer disease and Down syndrome, Proc. Natl. Acad. Sci. U. S. A. 82 (1985) 4245–4249.
[4] I. Grundke-Iqbal, K. Iqbal, Y.C. Tung, M. Quinlan, H.M. Wisniewski, L.I. Binder, Abnormal phosphorylation of the microtubule-associated protein τ (tau) in Alzheimer cytoskeletal pathology, Proc. Natl. Acad. Sci. U. S. A. 83 (1986) 4913–4917.
[5] F.M. Laferla, K.N. Green, S. Oddo, Intracellular amyloid-β in Alzheimer's disease, Nat. Rev. Neurosci. 8 (2007) 499–509.
[6] J. Näslund, V. Haroutunian, R. Mohs, K.L. Davis, P. Davies, P. Greengard, J.D. Buxbaum, Correlation between elevated levels of amyloid β-peptide in the brain and cognitive decline, JAMA 283 (2000) 1571–1577.
[7] M. Knobloch, U. Konietzko, D.C. Krebs, R.M. Nitsch, Intracellular Aβ and cognitive deficits precede β-amyloid deposition in transgenic arcAβ mice, Neurobiol. Aging 28 (2007) 1297–1306.
[8] G.K. Gouras, J. Tsai, J. Näslund, B. Vincent, M. Edgar, F. Checler, J.P. Greenfield, V. Haroutunian, J.D. Buxbaum, H. Xu, P. Greengard, N.R. Relkin, Intraneuronal Aβ42 accumulation in human brain, Am. J. Pathol. 156 (2000) 15–20.
[9] X. Hu, S.L. Crick, G. Bu, C. Frieden, R.V. Pappu, J.M. Lee, Amyloid seeds formed by cellular uptake, concentration, and aggregation of the amyloid-beta peptide, Proc. Natl. Acad. Sci. U. S. A. 106 (2009) 20324–20329.
[10] E. Wesen, G.D.M. Jeffries, M. Matson Dzebo, E.K. Esbjörner, Endocytic uptake of monomeric amyloid-beta peptides is clathrin- and dynamin-independent and results in selective accumulation of Abeta(1–42) compared to Abeta(1–40), Sci. Rep. 7 (2017) 2021.
[11] E.K. Esbjörner, F. Chan, E. Rees, M. Erdelyi, L.M. Luheshi, C.W. Bertoncini, C.F. Kaminski, C.M. Dobson, G.S. Kaminski Schierle, Direct observations of amyloid β self-assembly in live cells provide insights into differences in the kinetics of Aβ(1–40) and Aβ(1–42) aggregation, Chem. Biol. 21 (2014) 732–742.
[12] R.P. Friedrich, K. Tepper, R. Ronicke, M. Soom, M. Westermann, K. Reymann, C. Kaether, M. Fandrich, Mechanism of amyloid plaque formation suggests an intracellular basis of Aβ pathogenicity, Proc. Natl. Acad. Sci. U. S. A. 107 (2010) 1942–1947.
[13] A.D. Snow, J.P. Willmer, R. Kisilevsky, Sulfated glycosaminoglycans in Alzheimer's disease, Hum. Pathol. 18 (1987) 506–510.
[14] A.D. Snow, H. Mar, D. Nochlin, K. Kimata, M. Kato, S. Suzuki, J. Hassell, T.N. Wight, The presence of heparan sulfate proteoglycans in the neuritic plaques and congophilic angiopathy in Alzheimer's disease, Am. J. Pathol. 133 (1988) 456–463.
[15] J.H. Su, B.J. Cummings, C.W. Cotman, Localization of heparan sulfate glycosaminoglycan and proteoglycan core protein in aged brain and Alzheimer's disease, Neuroscience 51 (1992) 801–813.
[16] D.A. Dewitt, J. Silver, D.R. Canning, G. Perry, Chondroitin sulfate proteoglycans are associated with the lesions of Alzheimer's disease, Exp. Neurol. 121 (1993) 149–152.
[17] A.G. Woods, D.H. Cribbs, E.R. Whittemore, C.W. Cotman, Heparan sulfate and chondroitin sulfate glycosaminoglycan attenuate beta-amyloid(25–35) induced neurodegeneration in cultured hippocampal neurons, Brain Res. 697 (1995) 53–62.
[18] E. Sandwall, P. O'Callaghan, X. Zhang, U. Lindahl, L. Lannfelt, J.P. Li, Heparan sulfate mediates amyloid-beta internalization and cytotoxicity, Glycobiology 20 (2010) 533–541.
[19] G.M. Castillo, W. Lukito, T.N. Wight, A.D. Snow, The sulfate moieties of glycosaminoglycans are critical for the enhancement of beta-amyloid protein fibril formation, J. Neurochem. 72 (1999) 1681–1687.
[20] J. McLaurin, T. Franklin, X. Zhang, J. Deng, P.E. Fraser, Interactions of Alzheimer amyloid-beta peptides with glycosaminoglycans effects on fibril nucleation and growth, Eur. J. Biochem. 266 (1999) 1101–1110.
[21] G.M. Castillo, C. Ngo, J. Cummings, T.N. Wight, A.D. Snow, Perlecan binds to the beta-amyloid proteins (A beta) of Alzheimer's disease, accelerates A beta fibril formation, and maintains A beta fibril stability, J. Neurochem. 69 (1997) 2452–2465.
[22] D.J. Watson, A.D. Lander, D.J. Selkoe, Heparin-binding properties of the amyloidogenic peptides Abeta and amylin. Dependence on aggregation state and inhibition by Congo red, J. Biol. Chem. 272 (1997) 31617–31624.
[23] K.L. Stewart, E. Hughes, E.A. Yates, G.R. Akien, T.Y. Huang, M.A. Lima, T.R. Rudd, M. Guerrini, S.C. Hung, S.E. Radford, D.A. Middleton, Atomic details of the interactions of glycosaminoglycans with amyloid-beta fibrils, J. Am. Chem. Soc. 138 (2016) 8328–8331.

[24] C.C. Liu, N. Zhao, Y. Yamaguchi, J.R. Cirrito, T. Kanekiyo, D.M. Holtzman, G. Bu, Neuronal heparan sulfates promote amyloid pathology by modulating brain amyloid-beta clearance and aggregation in Alzheimer's disease, Sci. Transl. Med. 8 (2016) 332ra344.
[25] Z. Zhang, S. Ohtake-Niimi, K. Kadomatsu, K. Uchimura, Reduced molecular size and altered disaccharide composition of cerebral chondroitin sulfate upon Alzheimer's pathogenesis in mice, Nagoya J. Med. Sci. 78 (2016) 293–301.
[26] Y. Fu, J. Zhao, Y. Atagi, H.M. Nielsen, C.C. Liu, H. Zheng, M. Shinohara, T. Kanekiyo, G. Bu, Apolipoprotein E lipoprotein particles inhibit amyloid-β uptake through cell surface heparan sulphate proteoglycan, Mol. Neurodegener. 11 (2016).
[27] T. Kanekiyo, J. Zhang, Q. Liu, C.C. Liu, L. Zhang, G. Bu, Heparan sulphate proteoglycan and the low-density lipoprotein receptor-related protein 1 constitute major pathways for neuronal amyloid-beta uptake, J. Neurosci. 31 (2011) 1644–1651.
[28] J.D. Esko, T.E. Stewart, W.H. Taylor, Animal cell mutants defective in glycosaminoglycan biosynthesis, Proc. Natl. Acad. Sci. U. S. A. 82 (1985) 3197–3201.
[29] W.B. Stine Jr., K.N. Dahlgren, G.A. Krafft, M.J. Ladu, In vitro characterization of conditions for amyloid-beta peptide oligomerization and fibrillogenesis, J. Biol. Chem. 278 (2003) 11612–11622.
[30] J. Brison, D.S. Benoit, S. Muramoto, M. Robinson, P.S. Stayton, D.G. Castner, ToF-SIMS imaging and depth profiling of HeLa cells treated with bromodeoxyuridine, Surf. Interface Anal. 43 (2011) 354–357.
[31] K. Zou, D. Kim, A. Kakio, K. Byun, J.S. Gong, J. Kim, M. Kim, N. Sawamura, S. Nishimoto, K. Matsuzaki, B. Lee, K. Yanagisawa, M. Michikawa, Amyloid β-protein (Aβ)1–40 protects neurons from damage induced by Aβ1–42 in culture and in rat brain, J. Neurochem. 87 (2003) 609–619.
[32] J.T. Jarrett, E.P. Berger, P.T. Lansbury Jr., The carboxy terminus of the β amyloid protein is critical for the seeding of amyloid formation: implications for the pathogenesis of Alzheimer's disease, Biochemistry 32 (1993) 4693–4697.
[33] P.H. Weigel, J.A. Oka, Temperature dependence of endocytosis mediated by the asialoglycoprotein receptor in isolated rat hepatocytes. Evidence for two potentially rate-limiting steps, J. Biol. Chem. 256 (1981) 2615–2617.
[34] S. Kumari, S. Mg, S. Mayor, Endocytosis unplugged: multiple ways to enter the cell, Cell Res. 20 (2010) 256–275.
[35] C.K. Payne, S.A. Jones, C. Chen, X. Zhuang, Internalization and trafficking of cell surface proteoglycans and proteoglycan-binding ligands, Traffic 8 (2007) 389–401.
[36] I. Nakase, A. Tadokoro, N. Kawabata, T. Takeuchi, H. Katoh, K. Hiramoto, M. Negishi, M. Nomizu, Y. Sugiura, S. Futaki, Interaction of arginine-rich peptides with membrane-associated proteoglycans is crucial for induction of actin organization and macropinocytosis, Biochemistry 46 (2007) 492–501.
[37] L. Li, T. Wan, M. Wan, B. Liu, R. Cheng, R. Zhang, The effect of the size of fluorescent dextran on its endocytic pathway, Cell Biol. Int. 39 (2015) 531–539.
[38] R. Lundmark, G.J. Doherty, M.T. Howes, K. Cortese, Y. Vallis, R.G. Parton, H.T. McMahon, The GTPase-activating protein GRAF1 regulates the CLIC/GEEC endocytic pathway, Curr. Biol. 18 (2008) 1802–1808.
[39] H.L. Åmand, H.A. Rydberg, L.H. Fornander, P. Lincoln, B. Nordén, E.K. Esbjörner, Cell surface binding and uptake of arginine- and lysine-rich penetratin peptides in absence and presence of proteoglycans, Biochim. Biophys. Acta 1818 (2012) 2669–2678.
[40] S.G. Ostrowski, C.T. Van Bell, N. Winograd, A.G. Ewing, Mass spectrometric imaging of highly curved membranes during Tetrahymena mating, Science 305 (2004) 71–73.
[41] P. Sjövall, J. Lausmaa, H. Nygren, L. Carlsson, P. Malmberg, Imaging of membrane lipids in single cells by imprint-imaging time-of-flight secondary ion mass spectrometry, Anal. Chem. 75 (2003) 3429–3434.
[42] S.P. Mukherjee, B. Lazzaretto, K. Hultenby, L. Newman, A.F. Rodrigues, N. Lozano, K. Kostarelos, P. Malmberg, B. Fadeel, Graphene oxide elicits membrane lipid changes and neutrophil extracellular trap formation, Chem. 4 (2018) 334–358.
[43] K.M. Bolles, F. Cheng, J. Burk-Rafel, M. Dubey, D.M. Ratner, Imaging analysis of carbohydrate-modified surfaces using ToF-SIMS and SPRi, Materials (Basel) 3 (2010).
[44] D. Aoki, Y. Hanaya, T. Akita, Y. Matsushita, M. Yoshida, K. Kuroda, S. Yagami, R. Takama, K. Fukushima, Distribution of coniferin in freeze-fixed stem of Ginkgo biloba L. by cryo-TOF-SIMS/SEM, Sci. Rep. 6 (2016) 31525.
[45] S.I. Cohen, S. Linse, L.M. Luheshi, E. Hellstrand, D.A. White, L. Rajah, D.E. Otzen, M. Vendruscolo, C.M. Dobson, T.P. Knowles, Proliferation of amyloid-beta42 aggregates occurs through a secondary nucleation mechanism, Proc. Natl. Acad. Sci. U. S. A. 110 (2013) 9758–9763.
[46] G. Meisl, X. Yang, E. Hellstrand, B. Frohm, J.B. Kirkegaard, S.I. Cohen, C.M. Dobson, S. Linse, T.P. Knowles, Differences in nucleation behavior underlie the contrasting aggregation kinetics of the Aβ40 and Aβ42 peptides, Proc. Natl. Acad. Sci. U. S. A. 111 (2014) 9384–9389.
[47] S. Jin, N. Kedia, E. Illes-Toth, I. Haralampiev, S. Prisner, A. Herrmann, E.E. Wanker, J. Bieschke, Amyloid-beta(1–42) aggregation initiates its cellular uptake and cytotoxicity, J. Biol. Chem. 291 (2016) 19590–19606.
[48] J.S. Wadia, R.V. Stan, S.F. Dowdy, Transducible TAT-HA fusogenic peptide enhances escape of TAT-fusion proteins after lipid raft macropinocytosis, Nat. Med. 10 (2004) 310–315.
[49] H.L. Åmand, K. Fant, B. Norden, E.K. Esbjörner, Stimulated endocytosis in penetratin uptake: effect of arginine and lysine, Biochem. Biophys. Res. Commun. 371 (2008) 621–625.
[50] M.P. Lambert, A.K. Barlow, B.A. Chromy, C. Edwards, R. Freed, M. Liosatos, T.E. Morgan, I. Rozovsky, B. Trommer, K.L. Viola, P. Wals, C. Zhang, C.E. Finch, G.A. Krafft, W.L. Klein, Diffusible, nonfibrillar ligands derived from Abeta1–42 are potent central nervous system neurotoxins, Proc. Natl. Acad. Sci. U. S. A. 95 (1998) 6448–6453.
[51] P. Aran Terol, J.R. Kumita, S.C. Hook, C.M. Dobson, E.K. Esbjörner, Solvent exposure of Tyr10 as a probe of structural differences between monomeric and aggregated forms of the amyloid-beta peptide, Biochem. Biophys. Res. Commun. 468 (2015) 696–701.
[52] P. Narayan, A. Orte, R.W. Clarke, B. Bolognesi, S. Hook, K.A. Ganzinger, S. Meehan, M.R. Wilson, C.M. Dobson, D. Klenerman, The extracellular chaperone clusterin sequesters oligomeric forms of the amyloid-beta(1–40) peptide, Nat. Struct. Mol. Biol. 19 (2011) 79–83.
[53] S.D. Quinn, P.A. Dalgarno, R.T. Cameron, G.J. Hedley, C. Hacker, J.M. Lucocq, G.S. Baillie, I.D. Samuel, J.C. Penedo, Real-time probing of beta-amyloid self-assembly and inhibition using fluorescence self-quenching between neighbouring dyes, Mol. BioSyst. 10 (2014) 34–44.
[54] F. Cheng, K. Ruscher, L.A. Fransson, K. Mani, Non-toxic amyloid beta formed in the presence of glypican-1 or its deaminatively generated heparan sulfate degradation products, Glycobiology 23 (2013) 1510–1519.
[55] I. Benilova, E. Karran, B. De Strooper, The toxic Abeta oligomer and Alzheimer's disease: an emperor in need of clothes, Nat. Neurosci. 15 (2012) 349–357.
[56] A. Ziegler, J. Seelig, Contributions of glycosaminoglycan binding and clustering to the biological uptake of the nonamphipathic cell-penetrating peptide WR9, Biochemistry 50 (2011) 4650–4664.
[57] J. Huotari, A. Helenius, Endosome maturation, EMBO J. 30 (2011) 3481–3500.
[58] M. Matson Dzebo, A. Reymer, K. Fant, P. Lincoln, B. Norden, S. Rocha, Enhanced cellular uptake of antisecretory peptide AF-16 through proteoglycan binding, Biochemistry 53 (2014) 6566–6573.
[59] A.J. Yang, D. Chandswangbhuvana, L. Margol, C.G. Glabe, Loss of endosomal/lysosomal membrane impermeability is an early event in amyloid Abeta1–42 pathogenesis, J. Neurosci. Res. 52 (1998) 691–698.